Scientia Iranica D (2023) 30(3), 1085–1096

Sharif University of Technology
Scientia Iranica
Transactions D: Computer Science & Engineering and Electrical Engineering
http://scientiairanica.sharif.edu

C- and circular-shaped barriers optimization in a synchronous reluctance rotor for torque ripples minimization

M. Naeimi[a], R. Nasiri-Zarandi[b,*], and K. Abbaszadeh[a]

a. *Department of Electrical Engineering, K.N. Toosi University of Technology, Tehran, Iran.*
b. *Electrical Machine Group, Niroo Research Institute (NRI), Tehran, Iran.*

Received 29 November 2020; received in revised form 8 August 2021; accepted 20 September 2021

KEYWORDS
Synchronous Reluctance Motor (SynRM);
C-shaped barriers;
Circular barriers;
Particle Swarm Optimization (PSO) algorithm;
Torque ripple;
Average torque;
Finite Element Analysis (FEA).

Abstract. Due to the lack of magnets and suitable final price, Synchronous Reluctance Motors (SynRMs) are potential candidates for household electric appliances and so on. However, in general, they have a major drawback, i.e., high torque ripple. The optimized design of a synchronous reluctance rotor structure is presented for two different types of barrier shape with the aim of reducing the torque ripple and increasing the average torque. In this paper, optimization of rotor geometries with a fixed machine size for two types of C-shaped and circular barriers is investigated. Most of the rotor parameters such as the width of the iron parts as well as the width of the barriers along d and q axes are optimized by a new method using the Particle Swarm Optimization (PSO) algorithm. In addition, the angle of the end points for each barrier with constant rib and insulation factor are considered in the optimization process. Minimizing the torque ripple without losing or even increasing the average torque is the most critical optimization achievement. Two prototypes of the optimized rotor with the C-shaped and circular barriers were fabricated and experimentally compared. The results obtained from the 2D finite element simulation of the recommended machine conformed well to the experimental result.

1. Introduction

Recently, Synchronous Reluctance Motors (SynRMs) have notably attracted the attention of academicians owing to their various industrial applications such as pumps [1], electric vehicles [2,3], and elevators [4,5] due to their reduced maintenance costs, reduced manufacturing costs, and high efficiency. This process has encouraged further research on the optimization of rotor parameters and selection of rotor types with the aim of improving SynRM performance. In [1], studies on Flux Barrier (FB) machine and salient pole machine were carried out and compared. Further research works can be done on the number of FBs as well as the number of stator teeth. In [6], the effects of the geometric structure of six different rotors and two stators with a different number of slots on rotor iron losses were investigated, and the SynRM performance improvement was highlighted.

Among the main characteristics of SynRMs targeted for the design and optimization are the torque ripple [7], average torque, power factor improvement, and saliency ratio enhancement [8,9]. The number of the FBs [10] and their geometric shape [11] were also

*. *Corresponding author.*
E-mail address: Rnasirizarandi@nri.ac.ir (R. Nasiri-Zarandi)

doi: 10.24200/sci.2021.57254.5140

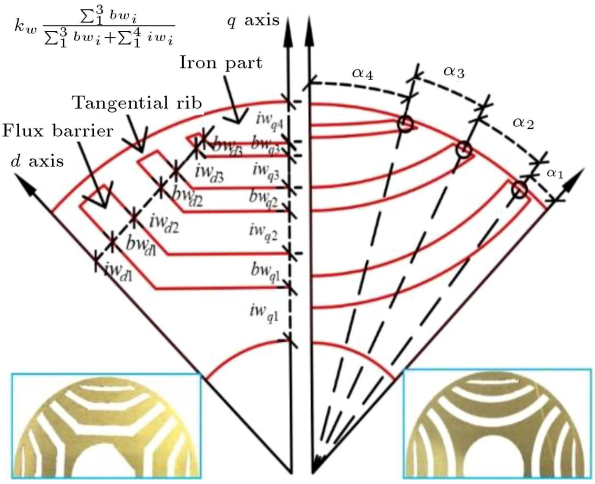

Figure 1. Parameters of the SynRM rotor with C-shape and circular barriers.

optimized to improve the SynRM output characteristics. However, the large number of rotor parameters and their connection to the output characteristics of the SynRM make the motor optimization almost challenging. For this reason, in a majority of such optimizations, all the geometric parameters of the rotor are not taken into account and instead, efforts are made to simplify the optimization and reduce the complexities by ignoring several optimization parameters [12] or reducing the number of FBs [13]. A cross-sectional view of the rotor with all geometry specifications in a sample SynRM is presented in Figure 1.

To date, different algorithms such as Genetic Algorithm (GA) [14,15], Differential Evolution (DE), and Design Of Experiments (DOE) [16] have been used to optimize the rotor of a SynRM and other types of electrical machine. These methods are selected based on the complexity of the objective function and type of the optimization function, i.e., single- or multi-objective. It should be noted that torque ripple optimization is studied by a GA [14]. To this end, first, three topological geometries for the rotor barriers were presented and then, optimization was performed for all three samples, and the results were compared. In [17], in addition to the optimization of the rotor's FBs to reduce torque ripple, the five examples of the feasible flux barrier tip shapes were investigated. In this optimization, however, the endpoints angles of the barriers (α) were ignored. In [18], the endpoints angle of the barriers' parameters (α) and magnetic insulation ratio (k_w) were used to optimize the torque ripple by a multi-objective DE algorithm. This method calculates the average torque and torque ripple based on the barriers' angles and finds a place for the endpoints' angles of the barriers to optimize the torque ripple. However, the mentioned method ignores the width of each barrier in optimization, which has a significant effect on reducing the ripple. In [19], the application of Finite Element Method (FEM) and GA, the width of the iron parts, and width of the FB was optimized with the aim of reducing torque ripple and repeatedly, the effect of the endpoints' angles of the barriers in reducing torque ripple was neglected.

In this paper, the optimized C-shaped and circular barriers of the SynRM are proposed to reduce the torque ripple while improving the average torque through the Particle Swarm Optimization (PSO) algorithm. To reduce the torque ripple in this optimization, most of the rotor parameters are used to determine the geometric structure of the rotor in the proposed method. Increasing the number of parameters ensures an accurate structure for the rotor mainly due to obtaining the precise shapes of the barriers and thickness of the iron parts. In the proposed optimization method, a number of rotor parameters such as the width of barriers along the d and q axes, width of the iron parts along the d and q axes, and endpoints angles of the barriers are taken into account with constant rib thickness and magnetic insulation ratio (k_w). This optimization generates a particular geometrical structure of the rotor that does not keep constant the width of the iron parts and the angle between the center and arm of the barriers. The geometric structure of the C-shaped barriers for maximum torque ripple reduction is changed into a circular shape after optimization. Then, the optimized C- and circular-shaped barriers along with the initial design are simulated using 2D FEM, and the comparisons are made. In the last section, two rotor prototypes with C-shaped and circular barriers are constructed and tested to verify the optimization result. In addition, the performances of the two rotor prototypes are compared to determine the one that best meets the proposed optimization objectives.

2. Basic of geometric barrier design

In the SynRM design method, the shape of the rotor barriers remarkably affects the design principles. The focus here is on optimizing the rotor FB and for this purpose, an induction motor's stator is used to reduce the manufacturing cost. Since the stator of the induction motors and SynRM are conceptually similar, a 1 Hp, 50 Hz, 400 V, 1500 rpm induction motor is selected as a sample machine. The main structural components of the sample induction motor are shown in Figure 2.

2.1. Conventional design of rotor geometric structure

The conventional design of the rotor is briefly described in this section [20,21]. In this method, the effects of saturation are ignored, while the Magneto Motive Force (MMF) waveform is considered sinusoidally. The width of the iron part is kept constant along the flux paths

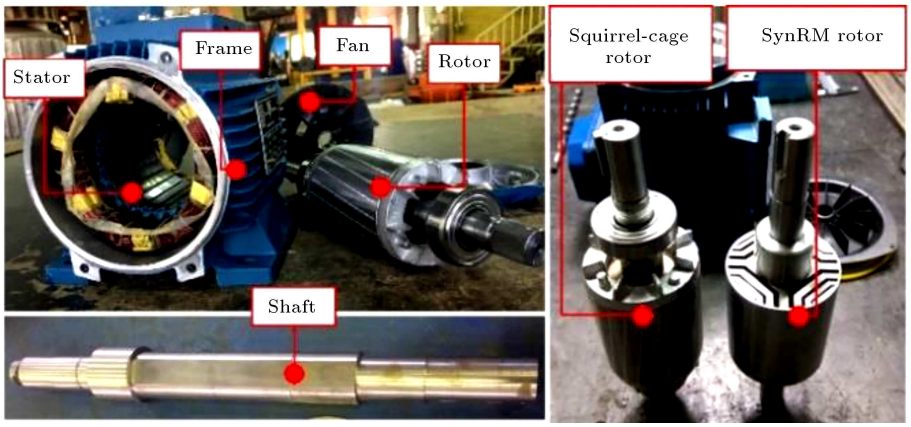

Figure 2. The procedure of disassembling of different parts of the induction motor.

Table 1. Specifications of different parts of the rotor before and after optimization (Figure 1).

Initial	Final	Parameter	Initial	Final	Parameter
α_1^*	5.625°	6.25°	bw_{q1}	3 mm	3.1 mm
α_2^*	17.189°	18.35°	bw_{q2}	2.15 mm	2.18 mm
α_3^*	28.125°	31.47°	bw_{q3}	1.16 mm	1.25 mm
α_4^*	39.53°	39.37°	bw_{d1}	2.87 mm	2.45 mm
iw_1	3.33 mm	3.12 mm	bw_{d2}	2 mm	1.85 mm
iw_2	6.137 mm	6.02 mm	bw_{d3}	1.08 mm	1.19 mm
iw_3	4.685 mm	6.64 mm	Air gap	0.5 mm	0.5 mm
iw_4	1.918 mm	1.89 mm	–	–	–

in the rotor to reach an equal flux density along the iron part. The iron part width (iw) is proportional to the average MMF along the d axis (F); in other words, the kth and hth segments can be written as Eq. (1). Followed by calculating the average MMF for each iron part and solving the equation set, the iron part width is obtained. Then, the method used hereafter for sizing of each barrier width (bw) refers to derivations given in [20]. Here, n_b represents the number of barriers and F_i the average MMF in the ith iron part. Also, D_{rotor}, D_{shaft}, and p are the outer diameter, and inner diameter, and number of rotor poles, respectively.

The geometrical structure of the rotor is determined via Eqs. (1)–(6), followed by calculating the width of the iron part and barriers. The conventional rotor design has some disadvantages, namely the primary design assumptions, use of limited number of barrier parameters, and non-optimization of the rotor parameters with a specific purpose. In the conventional design, different barriers in different shapes, such as C- and circular-shaped barriers, are ignored to reduce the torque ripple and the consequent effects are also neglected. In the next part, optimization will be done on the maximum number of rotor parameters for two different C- and circular-shaped geometric structures. The optimum dimensions of the rotor are presented in Table 1.

$$\frac{iw_k}{iw_h} = \frac{F_k}{F_h}, \tag{1}$$

$$F_i = \frac{\int_{\alpha_{b,i-1}}^{\alpha_{b,i}} \cos(p\alpha)d\alpha}{\alpha_{b,i} - \alpha_{b,i-1}} \quad \text{for} \quad i = 1, ..., n_b, \tag{2}$$

$$k_w = \frac{(D_{rotor} - D_{shaft}) - 2\sum_{k=1}^{n_b+1} iw_k}{2\sum_{k=1}^{n_b+1} iw_k}, \tag{3}$$

$$\begin{cases} F_{q,1} = 0 \\ F_{q,i} = \frac{\int_{\alpha_{b,i+1}}^{\alpha_{b,i}} \sin(p\alpha)d\alpha}{\alpha_{b,i} - \alpha_{b,i+1}} \quad \text{for} \quad i = 2, ..., n_b, \end{cases} \tag{4}$$

$$\Delta F_{i-1} = Fq_i - Fq_{i-1} \quad \text{for} \quad i = 2, ..., n_b, \tag{5}$$

$$\frac{bw_i}{bw_{i+1}} = \left(\frac{\Delta F_i}{\Delta F_{i+1}}\right)^2 \quad \text{for} \quad i = 2, ..., n_b + 1. \tag{6}$$

2.2. Main concept of the optimization of C-shape and circular barriers

Decreasing the torque ripple and improving the average torque of a SynRM by considering the rotor parameters have always been significant challenges facing the machine designers. The SynRM rotor is complicated

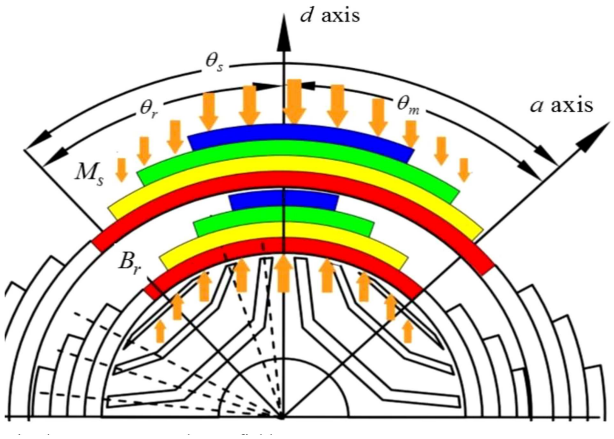

Figure 3. A graphical presentation of interaction between stator and rotor field.

due to the plurality of the parameters involved in the optimization design. The parameters should appear in the machine general torque equation to facilitate evaluation of the effect of rotor parameters in the machine torque profile. Then, the parameters should be determined to ensure the machine torque ripple reduction. The interaction between the stator's MMF and rotor's flux density leads to the electromagnetic torque of machine, as shown in Eq. (7). This interaction is graphically presented in Figure 3:

$$T(\theta_m) = k_t \int_0^{2\pi} B_r(\theta_m, \theta_r) M_s(\theta_m, \theta_r) d\theta_r = T_{av} + T_{rip}, \quad (7)$$

here, M_s, B_r, θ_m, θ_r, k_t, T_{av}, and T_{rip} are the stator MMF, rotor flux density, rotor position, angle in the rotor reference frame, motor geometry factor, average torque, and torque ripple, respectively. The coefficient k_t actually depends on the number of poles, the distribution coefficients of the winding, and stacking factor. As observed in Eq. (7), the average torque T_{av} has a constant value. The second phrase is the torque ripple, which is a function of the rotor position (θ_r) and rotor geometric structure. The stator's MMF typically possesses all the harmonics orders due to the distributed winding; therefore, the stator MMF waveform can be expressed as the Fourier expansion with different harmonic orders. According to the integral calculus, when two trigonometric functions with different harmonics are included in Eq. (7), only the components with the same harmonic take nonzero values. As a result, the torque ripple has a minimum value if the rotor flux density contains only the main harmonics (pure sinusoidal).

The objective of optimization is to provide a geometric structure for the rotor barriers to reduce the torque ripple. A majority of rotor parameters such as the barriers width, iron parts width, and endpoint angle of the barriers are used to achieve the closest sinusoidal shape for the rotor flux density. In addition, all the rotor optimization parameters are used for two types of barriers with different C- and circular-shaped structures, determining which optimization results will have the lowest torque ripple on which type of barrier shape.

3. Optimization method for barriers geometry

3.1. Proposed barriers shape optimization

The proposed optimization process is presented in the algorithm given in Figure 4. The challenge of optimization via PSO algorithms is how to define an objective function in terms of the maximum number of rotor parameters. In order for the torque ripple to decrease, the flux density shape must be purely sinusoidal. Rotor parameters should be used for this purpose. In the optimization, the endpoint angle of the barriers is used directly while the thicknesses of the iron parts and barriers are used indirectly. The

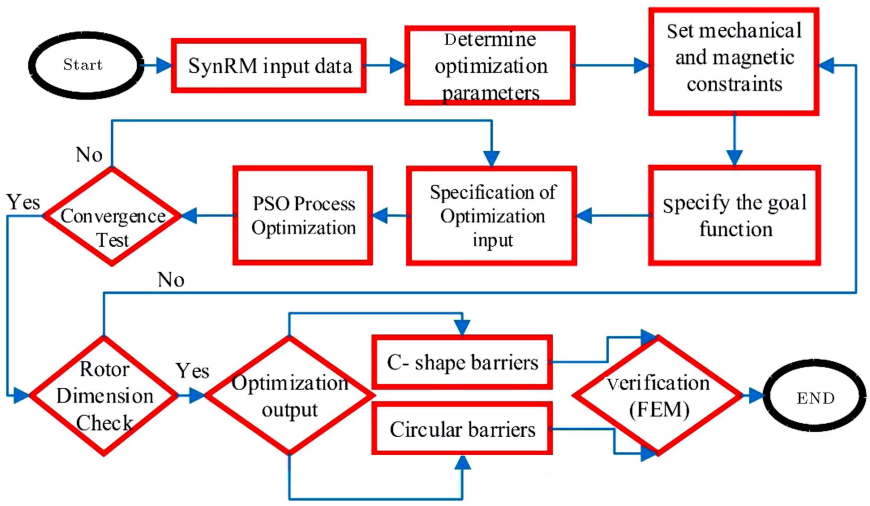

Figure 4. The proposed optimization algorithm.

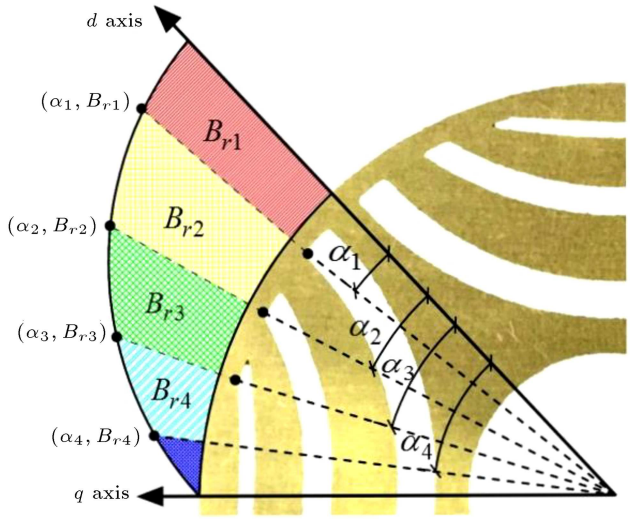

Figure 5. Each barrier and its adjacent iron part in the considered coordinates.

thicknesses of the iron parts will be modeled by the flux density that passes through them. In this regard, each barrier and the adjacent iron part make a special point in the 2D coordinates. The first is the endpoint angle of barriers, and the second is the value of the rotor flux density in the iron part adjacent to the barriers. Four 2D points are available with three barriers and four iron parts in each pole, as shown in Figure 5. The sinusoidal flux density must be achieved by these four points that determine the characteristics of the barriers and iron parts.

To this end, the flux density of the rotor is written in the form of a function f_x in terms of four mentioned coordinates, as shown in Eq. (8). These four points should be chosen such that the flux density waveform is as close as possible to the main harmonic. The defined function can be obtained from interpolating these four points by the optimization algorithm. The value of function f_x is reduced from the reference waveform f_{ref} for finding the best points. Then, the error function (RSME) should be minimized to zero or get closer to zero through the PSO algorithm.

$$B_r(\alpha_1, \alpha_2, \alpha_3, \alpha_4, B_{r1}, B_{r2}, B_{r3}, B_{r4}) = f_x((\alpha_1, B_{r1}), (\alpha_2, B_{r2}), (\alpha_3, B_{r3}), (\alpha_4, B_{r4})). \quad (8)$$

To find a function for several points, a curve fitting is conducted, as shown below:

$$MSE = \frac{1}{N}\sum_{K=1}^{N}(f_x - f_{ref})^2, \quad (9)$$

$$RMSE = \sqrt{MSE}, \quad (10)$$

where N is the number of rotor coordinations (α_k, B_{rk}) used for obtaining the best rotor geometric shape. The specific geometric structure is designed for the barriers and iron parts by minimizing the error function in optimization and obtaining the optimal parameters. In optimization, there are constraint functions to check the optimization performance. Based on the number of poles and dimensions of the rotor, these functions operate in such a way that the sum of the iron part and thickness of the barriers along the q axis does not exceed the rotor thickness value and the sum of all endpoint angles of the barriers does not exceed 45 degrees.

3.2. Optimization results and barrier geometric

In this investigation, the barrier parameters are considered as the optimization responses. Each particle in the optimization algorithm has all the optimization parameters, which are the geometric parameters of the barrier. Particles take values before and after optimization. The error value for each particle is extracted before and after optimization and is presented in the graphs of Figure 6. The final value of the particle indicates that the SynRM has still a small value of torque ripple and it is not zero. The average particle error values at the beginning and end of optimization are 0.15 and 0.015 Per-Unit (P.U), respectively. Figure 7 shows how the particles approach the reference waveform and, thus, reduce the error value of each particle. As observed, the particles in the four windows approach the reference waveform from different directions. Finally, four particles in each window are selected as the best points with the least error. The characteristics of each particle are the

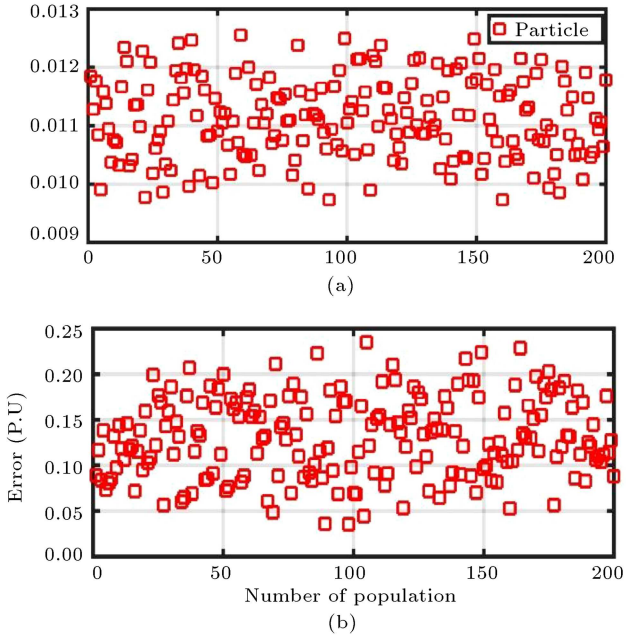

Figure 6. Error value per particle: (a) after and (b) before optimization.

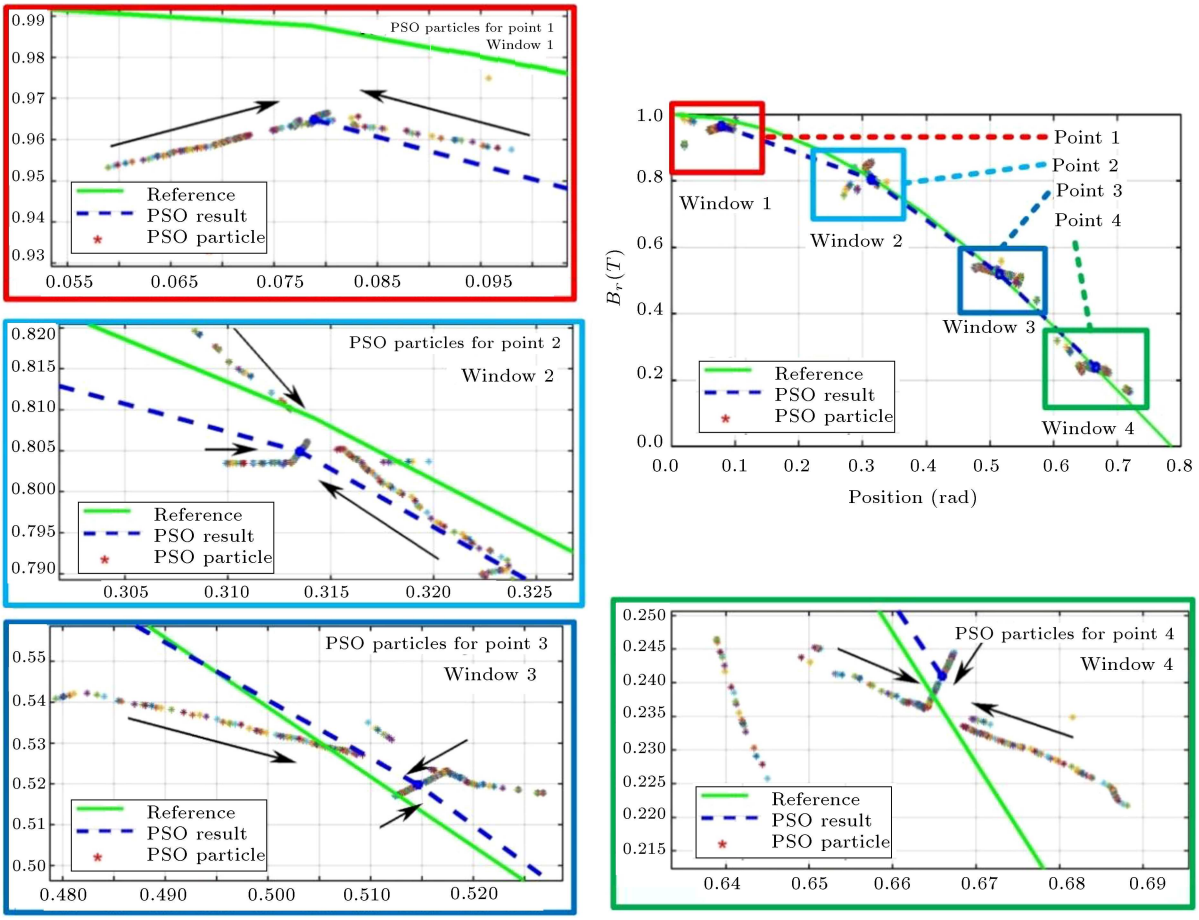

Figure 7. Overview of all optimization points with all the algorithm particles, comparison of reference graphs and graphs obtained from the optimization.

endpoint angles of the barriers and flux density of the iron part adjacent to the barrier. Once the information of the optimum particles is extracted, the optimum dimensions of the barriers can be obtained. The values of the optimized parameters such as the endpoint angles of the barriers, iron parts width, and barriers width along the d and q axes are presented in Table 1.

First, the width of the iron parts and barriers along the d and q axes should be adjusted to obtain the final structure of the C-shaped barrier of the rotor. Then, the endpoint angles of the barriers must be adjusted to the optimized angle, as shown in Figure 8. Further, to adjust the endpoint angles of the barriers, the points A, B, and C must be moved to the points A', B', and C'. The arm angle of the barriers in the directions $O'A$, $O''B$, and $O'''C$ with the center of O', O'', and O''' is opened to a point where the endpoints of the barriers are placed on A', B', and C'. The optimized C-shaped barriers are obtained by adjusting the endpoints of the barriers. As shown in Figure 9, each circular barrier consists of two circular curves. The optimum circular curve must be obtained according to the optimization results to achieve the optimum geometric structure of the rotor with a circular barrier. Given

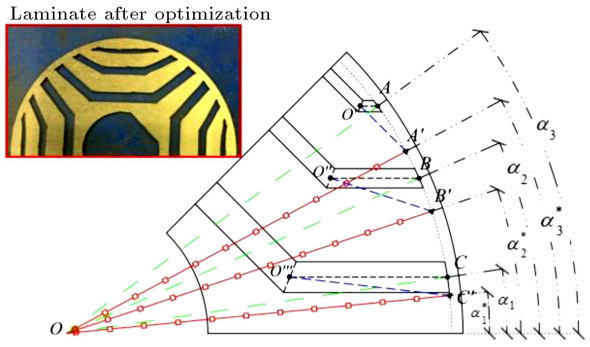

Figure 8. Steps of changing barriers end points to reach the optimum point.

that C-shape barriers obtained from optimization have an optimum structure, the circular curves that pass through the edge of these barriers are also optimum circular curves. Three points on the edges of the C-shaped barriers are used to form an optimum circular curve. Two of these three points are endpoints on the edge of the C-shaped barrier, and the other point is in the middle of the C-shaped barrier edge. Upon selecting two curves from the two edges of the C-shaped barriers, the optimal geometric structure of the

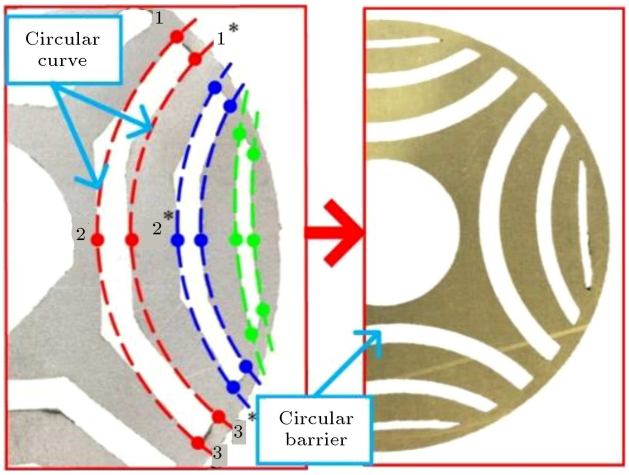

Figure 9. Changes of the C-shaped barrier to reach the circular barrier.

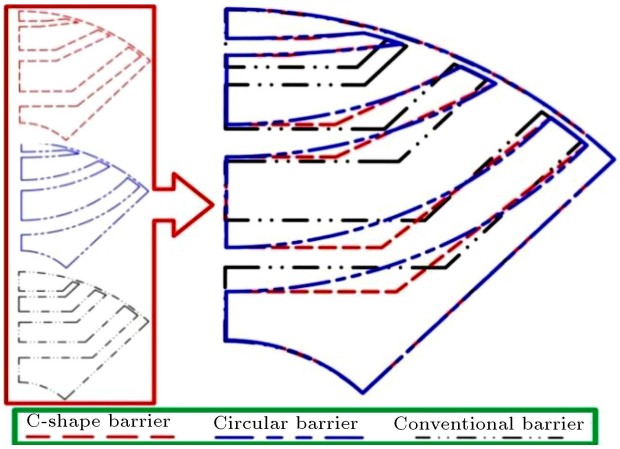

Figure 10. C-shape, circular, and conventional barriers of rotor.

rotor with circular barriers is obtained. The changes of the circular barriers compared to those of the C-shaped barriers are shown in Figure 10. As observed, the rotor shape of the C-shaped barriers, compared to conventional ones, has significantly changed. These changes can be observed at the endpoints and widths of the barriers and iron parts.

4. Result of experiments and comparisons

4.1. Finite Element Analysis (FEA) results

In order to validate the proposed optimization tool and developed process, a 1-Hp SynRM was simulated. Moreover, FEA was carried out to investigate the impact of the optimization on the C- and circular-shaped barriers. Ripple and average torque are improved by optimally changing the barrier parameters such as the endpoints angle and width of the barriers and the iron part. It is also shown that the shapes of the rotor with circular and C-shaped barriers have differences in torque ripple. The simulation results given in Table 2 show that the torque ripple for circular and C-shaped

Table 2. Optimization results of SynRM with different types of barrier.

Barrier type	Conventional	*C*-shape	Circular
Ave. torque	2.75 N.m	3.39 N.m	3.43 N.m
Torque ripple	21.81%	5.02%	4.80%
Power factor	50.2%	61.7%	63.3%

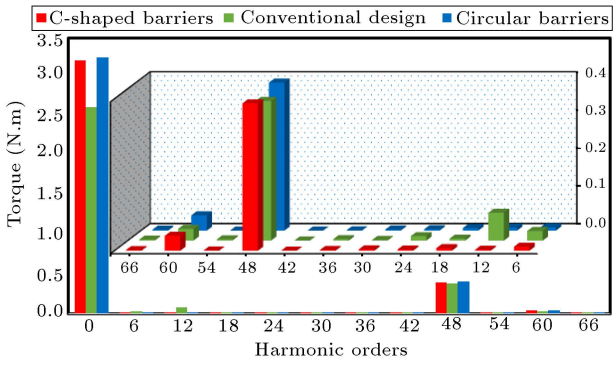

Figure 11. The torque harmonic spectrum of different types of barriers.

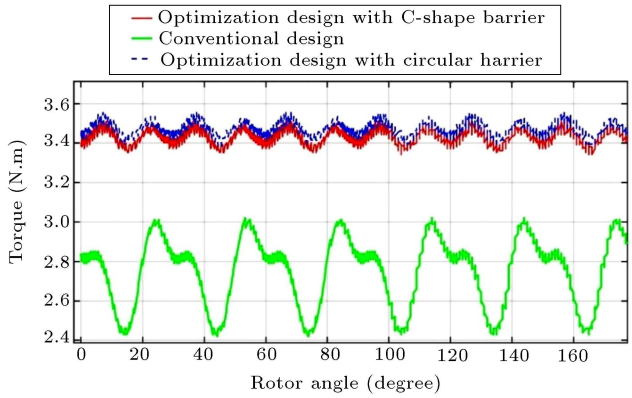

Figure 12. The torque versus rotor angle characteristic of the rotor with C-shape, circular, and conventional barriers.

barriers decreased by 17.01% and 16.79%, respectively, compared to conventional barrier. Figure 11 shows that the harmonics 6, 12, 24, 36, and 42 for both rotors with circular and C-shaped barriers were significantly reduced. Values for 6, 12, 24, 36, and 42 harmonics orders were reduced to 60%, 97%, 75%, 50%, and 66%, respectively, in the rotor with C-shape barriers. Besides, the rotor with circular barriers in the two harmonics 6 and 36 was reduced to 7% and 27%, respectively, compared to the rotor with C-shaped barriers. Also, the value of the torque main component increased as the torque harmonic orders decreased and the average torque value increased by 23.27% and 24.73% for C-shaped and circular barriers, respectively, compared to the conventional design. The output torque profile of the rotor with C-shape, circular, and conventional barriers is extracted and shown in Figure 12. As can be seen, the validation process by

FEM leads to acceptable results, which indicates the correctness of the proposed optimization method.

In order to investigate the accuracy of the simulation in terms of magnetic parameters, the contour plots of magnetic flux density for the rotor with optimized C-shaped, circular, and conventional machines are extracted and presented in Figure 13. As can be seen, the iron parts of all machines are not saturated and all components have a flux density close to 1.2 T, which is smaller than the knee point in B-H characteristic of the magnetic material. The ribs of SynRMs were saturated due to the cross-section of their small iron parts. It should be noted that the magnetic flux density in the ribs of the optimum C-shaped and circular barriers is around 1.8 T, which is less saturated than the conventional SynRM with 2 T of the magnetic flux density. It could be concluded that the proposed optimization leads to an acceptable design for this machine.

4.2. Prototype and test setup

In order to verify the proposed optimization method, two optimized rotors with circular and C-shaped barriers are prototyped. The rotor of SynRM with circular and C-shaped barriers is tested experimentally to validate the optimization performance and the FEA results. The M470-5A magnetic steel sheet is used and the manufacturing process is laser cutting. Figure 14 shows the rotor with C-shaped, circular, and conventional barriers. The experimental setup of Figure 15 is provided to measure the machine torque and evaluate the FEA results. The test setup includes a 4 kW control and driver package, dynamic transducer, mechanical couplings, and a Permanent Magnet Generator (PMG) as the static load. The SynRM is driven with general drive algorithm by considering the Voltage/frequency ratio constant in some steps. The V/f control method was implemented because the design and optimization were conducted by considering the stator of the machine the same as an existing induction motor. In addition, it must be noted that the SynRM is not a self-started motor. In this respect, the inverter setting is adjusted to 400 V, 50/60 HZ, 4 kW, 9 A as nominal power. Then, in five linear steps, the inverter injects power into machine. Also, a data acquisition system is implemented to extract all the test results. To ensure the correctness and validity of the measurements, the transducer calibration was performed at first and set at the maximum level of sensitivity before testing. Besides, before placing the rotor in the stator, a search coil was wrapped around a pole of the stator teeth to measure the air gap flux.

4.3. Torque characteristics

The experimental test for both SynRMs with an optimized rotor reveals the output torque characteristics including the torque ripple and the average torque. The

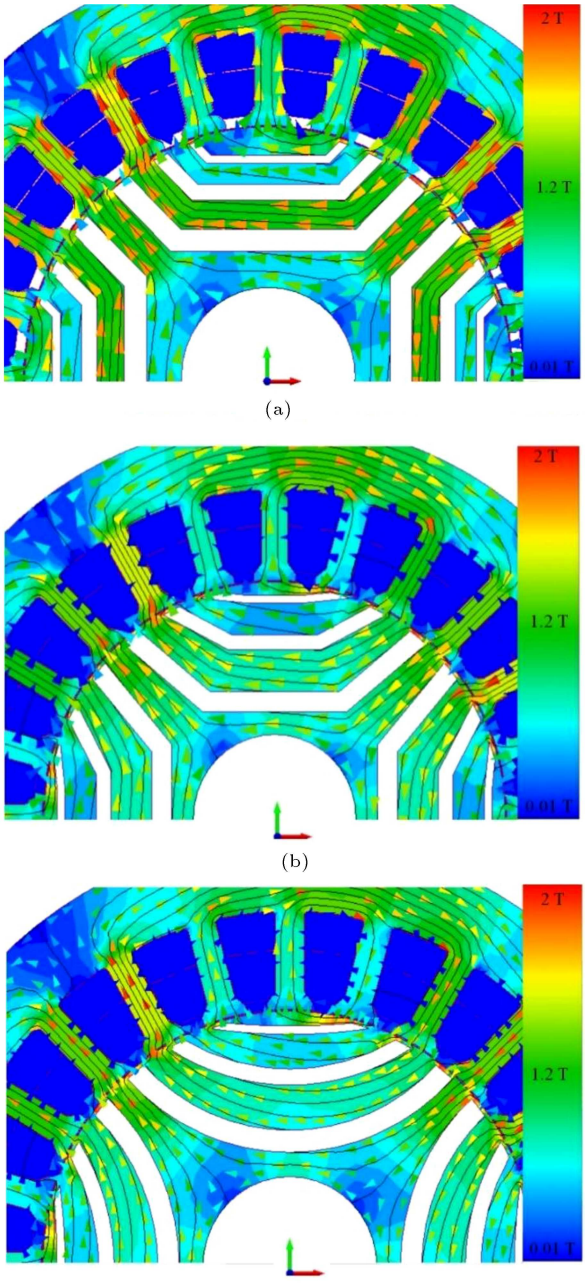

Figure 13. The magnetic flux density distribution in one pole of the rotor with (a) conventional barrier, (b) C-shape barrier, and (c) circular barrier.

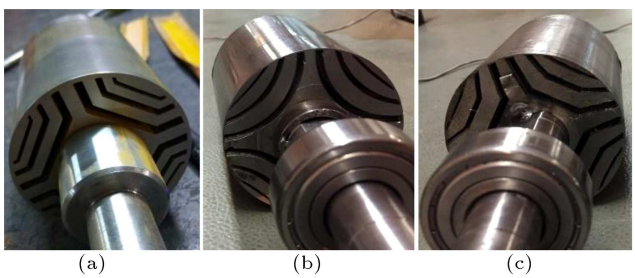

Figure 14. Rotors with (a) conventional, (b) circular, and (c) C-shaped barriers.

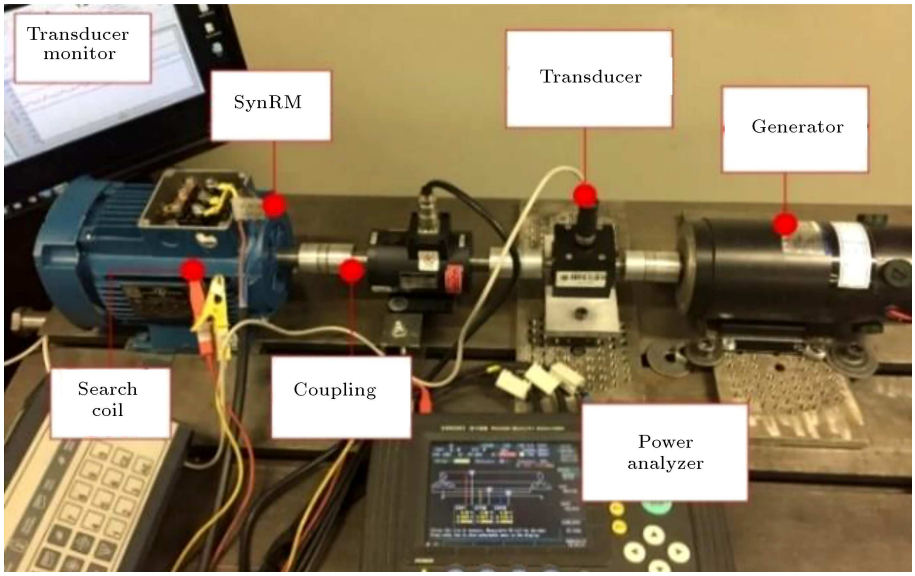

Figure 15. Experimental setup and measurement devices.

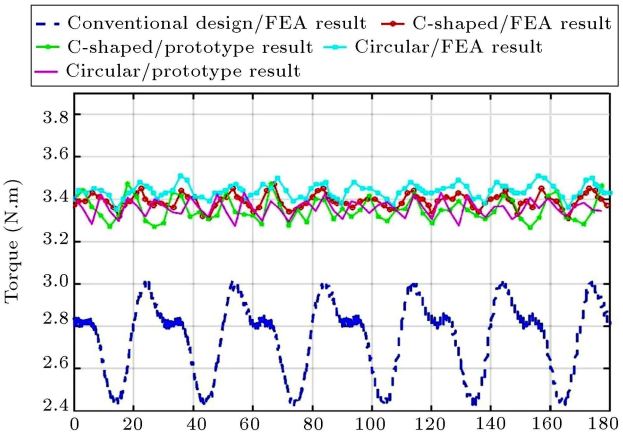

Figure 16. Comparison of simulation results for optimal and conventional rotor designs with prototype result.

torque ripple of SynRM rotor with C-shape and circular barriers was measured by dynamic transducer when the rotor shaft was coupled to PMG at a synchronous speed of 1500 r/min with ohmic load at nominal current. The adjustable-frequency AC drive was programmed to increase the motor speed up to 1500 r/min at nominal current in some predefined steps. As shown in Figure 16, the experimental test results for the two optimized rotors were significantly consistent with the FEA results. A minor difference was detected between the measurement data and the FEA due to mechanical fluctuations in the coupling (SynRM to transducer and transducer to PMG) and rotor manufacturing tolerance. According to Table 3, the experimental results show that after optimization, the torque ripple for the optimized rotor with the circular and C-shape barriers was reduced to 15.6% and 16.83%, respectively, compared to the conventional rotor.

Furthermore, after the rotor optimization process,

Table 3. Comparison of simulation and prototype results.

Barrier type/result type	Average torque	Torque ripple
Conventional/FEA result	2.75 N.m	21.81%
C-shaped/FEA result	3.38 N.m	5.02%
Circular/FEA result	3.43 N.m	4.80%
C-shaped/prototype result	3.35 N.m	6.21%
Circular/prototype result	3.36 N.m	4.98%

it is noticed that the average torque for both prototypes increased by 0.6 N.m compared to the conventional design. From the comparison between the two rotor prototypes in Table 3, it can be seen that the rotor with a circular barrier had 1.23% less torque ripple. Also, the average torque value increased to 0.01 Nm. Therefore, the rotor optimization goals with a circular structure were met better than those with the C-shaped barriers. Finally, experimental measurements for both optimized rotors demonstrate a significant improvement in SynRM torque ripple and average torque and confirm the simulation results, which can finally validate the accuracy of the proposed optimization algorithm.

4.4. Air gap flux characteristics

The shape of the air gap flux is an important indicator in determining the torque ripple. The torque ripple decreased considerably when the air gap flux waveform became closer to pure sinusoidal waveform. This goal was achieved by optimizing the parameters of synchronous reluctance rotor including the endpoint angles of barriers and the thickness of the iron parts and the barriers. To extract the air gap flux waveform in one rotor pole, a search coil with three turns of winding was wrapped around the six stator teeth

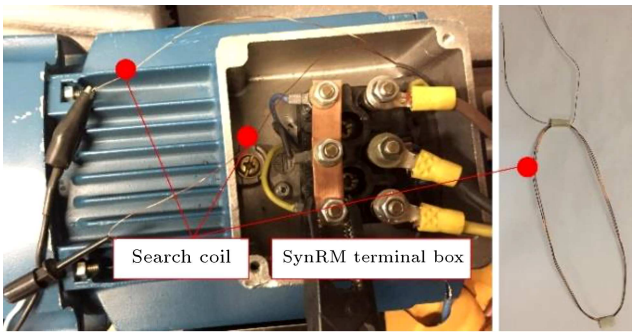

Figure 17. Search coil under a pole of SynRM.

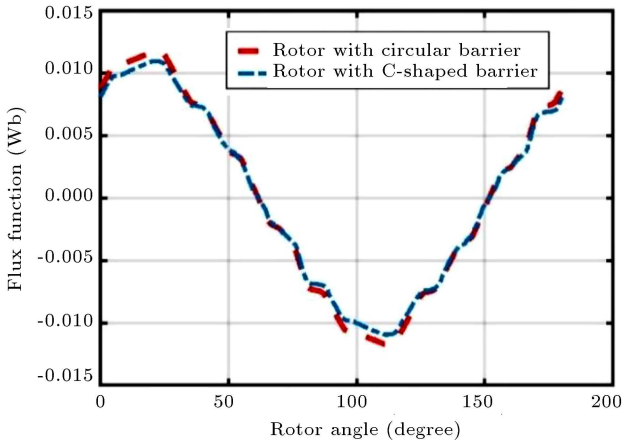

Figure 18. Air gap flux function under a pole of SynRM prototypes.

(equivalent to 1 pole) and connected to measurement tools (Figure 17). The waveform of induced voltage in the search coil was measured after starting synchronous reluctance at a nominal speed. Induced voltages waveform allows determining the air gap magnetic flux based on Faraday's Law. According to Figure 18, the flux waveform for the rotor with circular and C-shaped barriers was compared. As can be seen in Figure 18, the flux waveform for both rotors was as close to pure sinusoidal as possible. Therefore, the goal of optimization was achieved by optimizing the geometric shape of barriers and iron parts. On the other hand, the flux waveform for the rotor with a circular barrier was more uniform and closer to the pure sinusoidal. For this reason, the torque ripple for the rotor with circular barriers was less than the rotor with C-barriers, as can be observed in Table 3, in which the torque ripple in the experimental results was obtained. Of note, the main component of the air gap flux was an essential item for average electromagnetic torque generation. Table 3 shows 0.6 N.m increase in the average torque of the prototyped machines compared to the conventional design. Therefore, the SynRM with an optimized rotor had a higher main component of air gap flux that contributed to the useful torque generation. Consequently, in the case of the machine with the same size, the average torque of SynRM rotor with C-shaped and circular barriers was higher than that of the conventional SynRM in which the torque ripple declined considerably.

5. Conclusion

In this paper, the proposed optimization algorithm optimized the geometric structure of rotor barriers of Synchronous Reluctance Motor (SynRM) by using the possible rotor parameters to achieve the lowest torque ripple while increasing the average torque. Also, the results of optimization were performed on two types of rotors with circular and C-shaped barriers. By optimizing the geometry of the rotor barriers, parameters such as the endpoints angle of barriers and the width of barriers and iron parts changed dramatically, compared to the conventional rotor. Initially, the Finite Element Analysis (FEA) results of three rotors of SynRMs with conventional, circular, and C-shaped barriers were obtained. The results revealed that the FEA of the proposed SynRMs was valid and there was acceptable agreement between the FEA and optimization for reducing torque ripple. The torque ripple in the FEA for the rotor with the circular and C-shaped barriers was reduced by 17.01% and 16.79%, respectively, compared to a conventional rotor. Then, to evaluate the simulation results and confirm the optimization performance for rotor barriers, two prototypes of the optimized rotor with circular and C-shaped barriers were manufactured and tested in nominal conditions. The measurement results confirmed the simulation accuracy and optimization with a slight deviation. The torque ripple in the experimental test for the rotor with circular and C-shaped barriers improved by 16.83% and 15.6%, respectively. Another achievement of the optimization was that the average torque for the optimized rotor was increased to 0.6 Nm. Finally, based on the simulation results and measurement data, it was seen that the optimized rotor with the circular barrier fulfilled the optimization goals more than the optimized rotor with C-shaped barriers.

References

1. Oliveira, F. and Ukil, A. "Energy efficiency in variable speed centrifugal chiller systems driven by synchronous reluctance motors", *2018 IEEE Innovative Smart Grid Technologies - Asia (ISGT Asia)*, Singapore, pp. 340–344 (2018).
2. Hofer, M., Nikowitz, M., and Schrödl, M. "Comparative analysis of salient pole and flux barrier rotor for synchronous reluctance machines including flux weakening range", *The Journal of Engineering*, **2019**(17), pp. 4055–4059 (2019).
3. Salehinia, S.R., Afjei, E., and Hekmati, A. "Analytical method to optimum design of synchronous reluctance

motor for electric scooter application", *Scientia Iranica*, **29**(5), pp. 2537–2551 (2021).

4. Diao, X., Zhu, H., Qin, Y., et al. "Torque ripple minimization for bearingless synchronous reluctance motor", *IEEE Transactions on Applied Superconductivity*, **28**(3), pp. 1–5 (2018).

5. Li, J., Xin, M., Fan, Z., et al. "Design and experimental evaluation of a 12 kW large synchronous reluctance motor and control system for elevator traction", *IEEE Access*, **8**, pp. 34256–34264 (2020).

6. Castagnaro, E., Bacco, G., and Bianchi, N. "Impact of geometry on the rotor iron losses in synchronous reluctance motors", *IEEE Transactions on Industry Applications*, **55**(6), pp. 5865–5872 (2019).

7. Yan, D., Xia, C., Guo, L., et al. "Design and analysis for torque ripple reduction in synchronous reluctance machine", *2018 IEEE International Magnetics Conference (INTERMAG)*, Singapore, pp. 1–1 (2018).

8. Chai, W., Zhao, W., and Kwon, B. "Optimal design of wound field synchronous reluctance machines to improve torque by increasing the saliency ratio", *IEEE Transactions on Magnetics*, **53**(11), pp. 1–4 (2017).

9. Staton, D.A., Miller, T.J.E., and Wood, S.E. "Maximising the saliency ratio of the synchronous reluctance motor", *IEE Proceedings B - Electric Power Applications*, **140**(4), pp. 249–259 (1993).

10. Bacco, G. and Bianchi, N. "Design criteria of flux-barriers in synchronous reluctance machines", *IEEE Transactions on Industry Applications*, **55**(3), pp. 2490–2498 (2019).

11. Bianchi, N., Bolognani, S., Bon, D., et al. "Rotor flux-barrier design for torque ripple reduction in synchronous reluctance and PM-assisted synchronous reluctance motors", *IEEE Transactions on Industry Applications*, **45**(3), pp. 921–928 (2009).

12. Palmieri, M., Cascella, G.L., and Cupertino, F. "Design methodologies for the output power maximisation of synchronous reluctance machines", *IET Electric Power Applications*, **13**(8), pp. 1131–1140 (2019).

13. Mohammadi, M.H., Rahman, T., Silva, R., et al. "A computationally efficient algorithm for rotor design optimization of synchronous reluctance machines", *IEEE Transactions on Magnetics*, **52**(3), pp. 1–4 (2016).

14. Pellegrino, G., Cupertino, F., and Gerada, C. "Automatic design of synchronous reluctance motors focusing on barrier shape optimization", *IEEE Transactions on Industry Applications*, **51**(2), pp. 1465–1474 (2015).

15. Alemi-Rostami, M., Rezazadeh, G., Alipour-Sarabi, R., et al. "Design and optimization of a large-scale permanent magnet synchronous generator", *Scientia Iranica*, **29**(1), pp. 217–229 (2019).

16. Nasiri-Zarandi, R., Ajamloo, A.M., and Abbaszadeh, K. "Design optimization of a transverse flux halbach-array PM generator for direct drive wind turbines", *IEEE Transactions on Energy Conversion*, **35**(3), pp. 1485–1493 (2020).

17. Howard, E., Kamper, M.J., and Gerber, S. "Asymmetric flux barrier and skew design optimization of reluctance synchronous machines", *IEEE Transactions on Industry Applications*, **51**(5), pp. 3751–3760 (2015).

18. Babetto, C., Bacco, G., and Bianchi, N. "Synchronous reluctance machine optimization for high speed applications", *IEEE Transactions on Energy Conversion*, **33**(3), pp. 1266–1273 (2018).

19. Boztas, G., Aydogmus, O., Caner, M., et al. "Design, optimisation and implementation of low-voltage synchronous reluctance motor for solar-powered systems", *IET Power Electronics*, **12**(7), pp. 1679–1685 (2019).

20. Moghaddam, R.R. "Synchronous reluctance machine SynRM in variable speed drives VSD applications", Ph.D. Dissertation, KTH School of Electrical Engineering (2011).

21. Mahmoud, H., Bacco, G., Degano, M., et al. "Synchronous reluctance motor iron losses: Considering machine nonlinearity at MTPA, FW, and MTPV operating conditions", *IEEE Transactions on Energy Conversion*, **33**(3), pp. 1402–1410 (2018).

Biographies

Mohammadreza Naeimi was born in Tehran, Iran. He received the BS degree in Shahid Beheshti University, Tehran, Iran in 2017 and the MS degree in Electrical Engineering from the K. N. Toosi University of Technology, Tehran, Iran in 2019. He has recently started the PhD degree at the Electrical Engineering Department, K. N. Toosi University of Technology, Tehran, Iran. His current research interests include design, modeling, FEA, optimization, prototyping, and control of electric machines.

Reza Nasiri-Zarandi received the BS degree in Electrical Engineering from K. N. Toosi University of Technology, Tehran, Iran in 2008 and the MS degree in Electrical Engineering jointly with Amir Kabir University of Technology, Tehran, Iran in 2010. He received the PhD degree in Electrical Engineering and Energy jointly with Amir Kabir University of Technology, Tehran, Iran and the Polytechnic University of Turin, Turin, Italy. He is currently an Assistant Professor in the Electrical Machine Group, Niroo Research Institute (NRI), Tehran, Iran. His research interests include design, modeling, FEA, optimization, and drive of rotary electric machines and power electronics.

Karim Abbaszadeh received the BS degree in Communication Engineering from K. N. Toosi University

of Technology, Tehran, Iran in 1991 as well as MS and PhD degrees in Electrical Engineering from Amir Kabir University of Technology, Tehran, Iran in 1997 and 2000, respectively. From 2001 to 2003, he was a Research Assistant with the Department of Electrical Engineering, Texas A&M University, College Station, TX, USA. He is currently a Professor at the Department of Electrical Engineering, K. N. Toosi University of Technology. His research interests include power electronic and dc-dc and dc-ac converters, electric machinery, variable-speed drives, and propulsion applications.